Computational analysis of effects of external carotid artery flow and occlusion on adverse carotid bifurcation hemodynamics

Sinjae Hyun, PhD,[a] Clement Kleinstreuer, PhD,[b] and **Joseph P. Archie, Jr, PhD, MD,[b]** *Macon, Ga; and Raleigh, NC*

Objective: **This is a computational analysis of the effects of external carotid artery (ECA) flow, waveform, and occlusion geometry on two hemodynamic wall parameters associated with intimal hyperplasia and atherosclerosis.**
Study design: **Transient three-dimensional fluid mechanics analysis was applied to a standard carotid artery bifurcation. Mean internal carotid artery (ICA) flow was maintained at 236 mL/min with a normal waveform. ECA flow was increased from zero to 151 mL/min (64% of ICA flow) with both a normal biphasic waveform and a damped waveform. Geometry of five ECA occlusions was studied: distal, proximal stump, smooth, smooth without carotid sinus, and optimal reconstruction.**
Primary outcome measures: **Two time-averaged and area-averaged hemodynamic wall parameters were computed from the velocity and wall shear stress (WSS) solutions, ie, wall shear stress angle gradient (WSSAG) and oscillatory shear index (OSI). Both local and area-averaged hemodynamic wall parameters were computed for the distal common carotid artery (CCA) and the proximal ICA.**
Results: **When ECA flow with a normal waveform is increased from zero to 151 mL/min, area-averaged WSS values increase in the CCA, from 3.0 to 4.4 dynes/cm^2 (46%), and in the ICA, from 16.5 to 17.1 dynes/cm^2 (4%); minimum local WSS values in the carotid sinus remain less than 1 dyne/cm^2; maximum local values of WSSAG and OSI are observed in the carotid sinus and increase from 3.5 to 9.1 radian/cm (160%) and 0.23 to 0.46 (100%), respectively; CCA plus ICA area-averaged WSSAG increases by 52%, and OSI increases by 144%; and damping of the ECA waveform has little effect on local or area-averaged WSSAG but reduces OSI to 68%. When the ECA is occluded, the minimum local WSS in the carotid sinus is less than 1 dyne/cm^2. However, if the carotid sinus is removed or the CCA-ICA geometry hemodynamically optimized, the minimum WSS is approximately 4 dynes/cm^2. Similarly, eliminating the carotid sinus markedly reduces local maximum WSSAG, from 3.0-3.5 radian/cm to 0.3 radian/cm, and reduces local maximum OSI from 0.22-0.49 to 0.04. Area-averaged WSSAG and OSI over the CCA and ICA are reduced by approximately 50% with elimination of the carotid sinus.**
Conclusions: **The degree of adverse carotid bifurcation hemodynamics as measured with WSSAG and OSI is directly proportional to ECA flow. The marked difference in normal ICA and ECA flow waveforms does not contribute to adverse wall hemodynamics. Location of an ECA occlusion (distal, proximal, stump, smooth) does not affect adverse carotid hemodynamics; however, marked improvement is obtained with elimination of the carotid sinus. (J Vasc Surg 2003;37: 1248-54.)**

The extracranial carotid bifurcation is a frequent locus of stenosis due to atherosclerosis or restenosis, because of myointimal proliferation after carotid endarterectomy (CEA). It is generally accepted that the carotid bulb geometry produces adverse hemodynamics in the form of low wall shear stress (WSS) and high wall shear stress gradients and that these disturbed blood flow parameters have a major role in the cause of intimal hyperplasia and atherosclosis.[1-3] Two characteristics that make the carotid bifurcation somewhat unique are the different blood flow requirements and waveforms of the internal carotid artery (ICA) and the external carotid artery (ECA). Cerebral blood flow is normally closely autoregulated to provide cerebral flow of 50 to 55 mL/min/100 g.[4] The ICA has a relatively constant blood flow, with a pulsatile waveform characterized by high diastolic flow, similar to that in solid organs such as the kidney. In contrast, ECA flow can be highly variable both between and within individuals and generally has a biphasic waveform with little diastolic flow, similar to resting upper and lower extremity arterial flow. Both the variability in ICA and ECA flow ratios and the quite different pulsatile flow waveforms may be important components of hemodynamically generated adverse WSS, as well as its directional change and gradients in the carotid bifurcation. A second closely related problem is the possible adverse effect of ECA flow and waveform on recurrent stenosis after CEA and perhaps even after angioplasty and stenting. Management of ECA stenosis during routine CEA is controversial, in part because of high residual stenosis rate as well as early and late recurrent stenosis rates.[5] Thus some surgeons have recommended leaving the dis-

From the [a]Department of Biomedical Engineering, Mercer University, and the [b]Department of Mechanical and Aerospace Engineering, North Carolina State University.
Competition of interest: none.
Correspondence: Joseph P. Archie, Jr, MD, 2309 Woodrow Dr, Raleigh NC 27609 (e-mail: jparchie@aol.com).

0741-5214/2003/$30.00 + 0
doi:10.1016/S0741-5214(02)75326-3

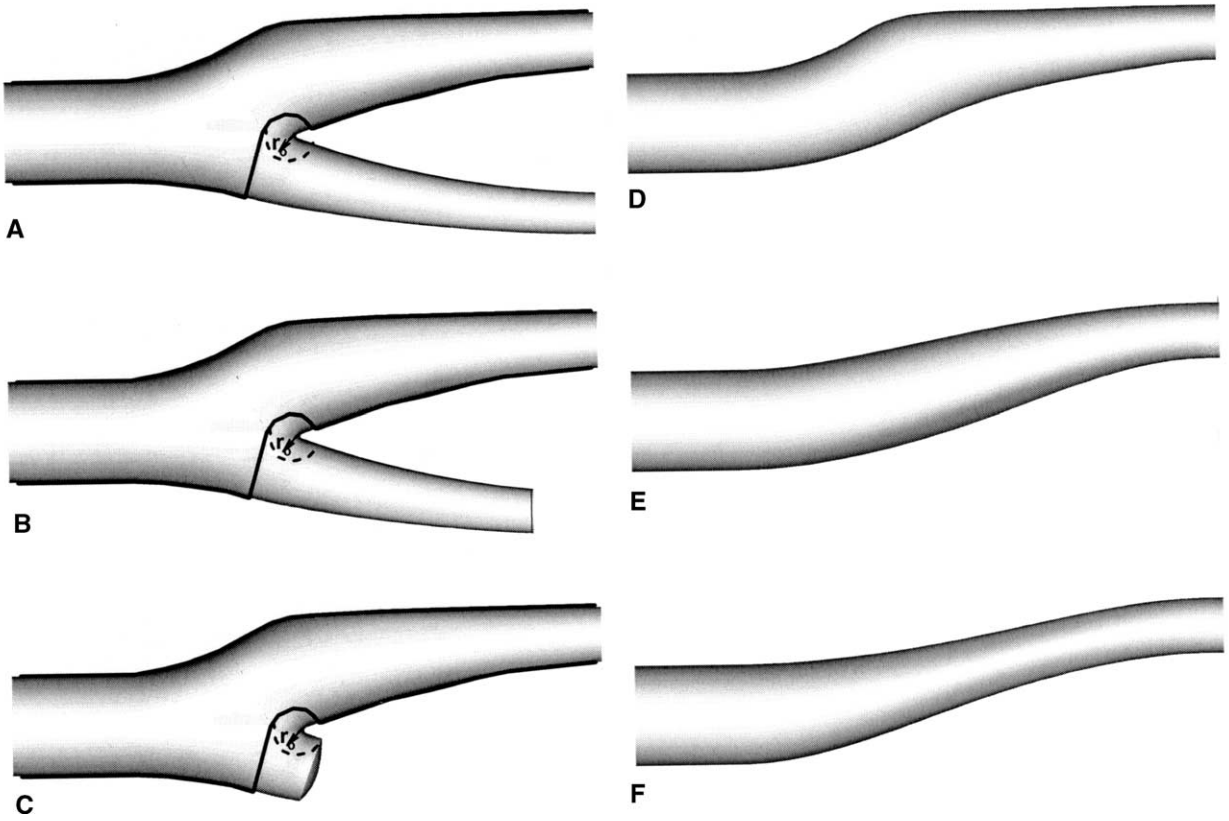

Fig 1. Occlusion geometry for six carotid bifurcations studied. **A**, Normal carotid artery bifurcation geometry. **B**, Distal ECA occlusion. **C**, Proximal stump carotid occlusion. **D**, Proximal smooth ECA occlusion. **E**, Proximal smooth ECA occlusion without carotid sinus. **F**, Optimal reconstruction excluding ECA. In **A**-**C**, divider and ECA wall surfaces excluded from computational analysis are shown.

eased ECA intact during CEA.[6] Although an isolated ECA occlusion is associated with a low complication rate, the question and advisability of excluding the ECA during CEA or other invasive procedures is of interest.

This study addresses these questions and issues. Computational simulation and analysis are used to investigate the effect of ECA flow, waveform, and occlusion geometry on adverse carotid bifurcation hemodynamics.

METHODS

Carotid artery geometry. A standard three-dimensional rigid and smooth-walled carotid bifurcation[7] (Fig 1, *A*) was used to compute flow velocity, as well as WSS and its spatial changes when the ECA was patent. The same geometry was used for distal ECA occlusion (Fig 1, *B*). This geometry was modified to produce distal occlusion, proximal stump occlusion, and proximal smooth occlusion (Fig 1, *B-D*). Geometry of two additional ECA exclusions were also studied, ie, absence of the carotid bulb or sinus (Fig 1, *E*), as well as geometry optimized by varying the geometric taper and curvature to produce the lowest adverse hemodynamics (Fig 1, *F*). The model has a proximal common carotid artery (CCA) diameter of 8 mm, a distal ICA diameter of 5.8. mm and a distal ECA diameter of 4.8 mm. Centerline axial length is about 20 mm for the CCA and about 30 mm for the ICA.

Flow conditions and equations. For all studies, mean ICA flow was maintained at 236 mL/min with a normal waveform. ECA flow was increased in five increments from zero to 151 mL/min (64% of ICA flow). At the inlet to the CCA, fully developed transient velocity profiles were used. Two ECA waveforms were used, ie, a normal biphasic waveform[8] and a damped waveform, with the same profile as that of the ICA (Fig 2, *B*). The damped ECA flow waveform was used for two reasons. First, we tested the hypothesis that the marked differences in normal ICA flow waveform (which has high diastolic flow, similar to that of the arterial supply to solid organs) and normal ECA flow waveform (which has essentially no diastolic flow, similar to resting extremity flow waveforms) have an adverse effect on carotid bifurcation hemodynamics. This may be expected because under normal flow conditions flow bifurcates into the ICA and ECA, but during diastole essentially all flow goes to the ICA. A damped ECA waveform similar to that of the ICA may improve the hemodynamics. The second reason to evaluate a damped ECA waveform was to mimic

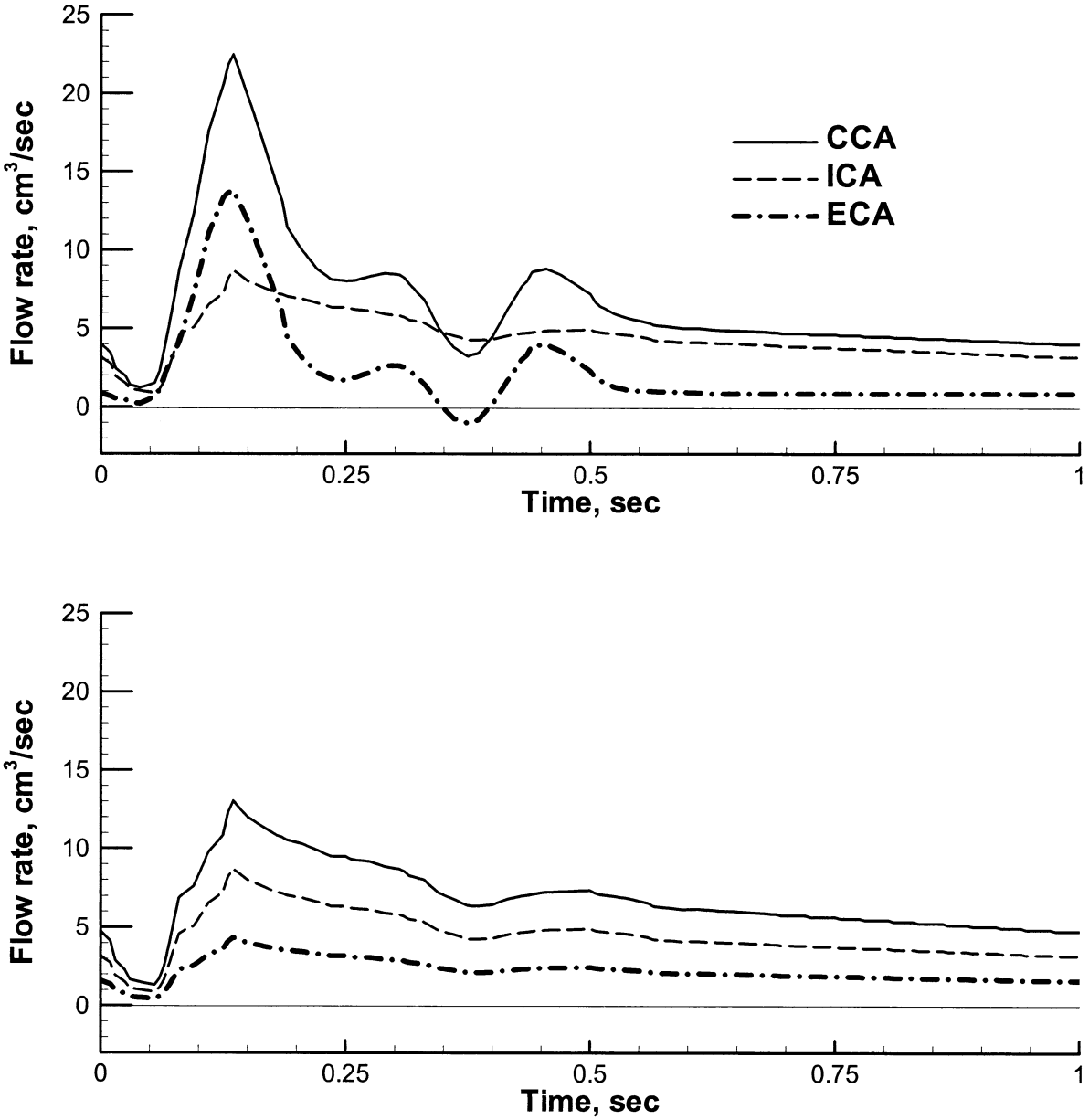

Fig 2. Volume time flow waveforms when ratio of ECA flow to ICA flow is 0.5. **A**, Normal waveforms. **B**, Damped ECA waveform with same profile as normal ICA waveform.

the effect of high-grade distal ECA stenosis. This cannot be done by adding ECA stenosis greater than 60%, because of the onset of turbulence, not considered here. Laminar three-dimensional incompressible non-Newtonian fluid flow was approximated with an extended Casson fluid model for hematocrit 40%.[9] Mean inlet Reynolds number was 457, and frequency was 1 cycle/sec. The governing equations were the continuity equation, ensuring conservation of mass, and the Navier-Stokes equation of fluid motion, ensuring conservation of linear momentum. Auxiliary boundary conditions with no fluid slip at the walls were applied in a manner to match the physiologic conditions shown in Fig 2. Fully developed transient Womersley velocity profiles were applied to the CCA inlet and to the ICA outlet, and a zero pressure outlet condition was selected for the ECA.

Computational simulation and analysis. Computations were performed with a validated finite volume-based algorithm CFX 4.4 with the SIMPLEC algorithm for pressure correction[10] and an algebraic multigrid scheme for solving the discretized Navier-Stokes equations on structured meshes and speedup of the iterations.[11,12] The com-

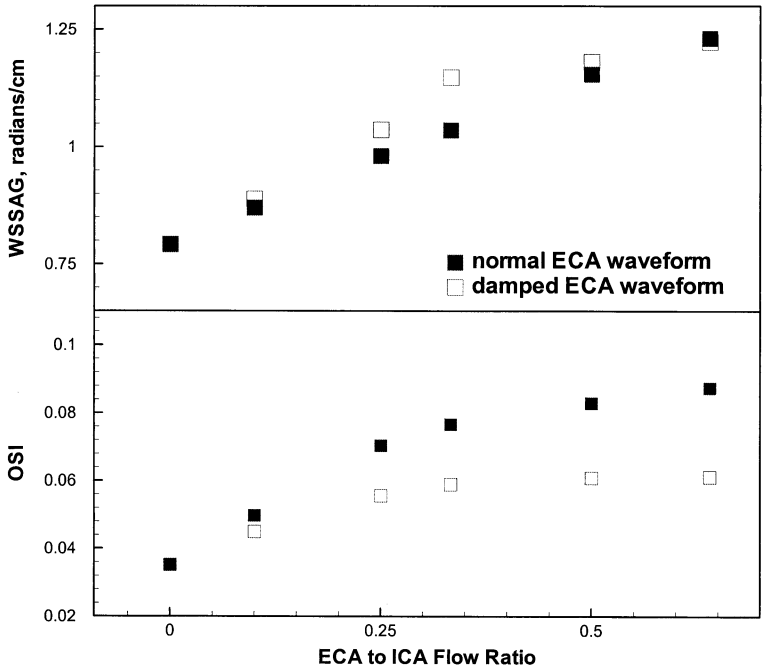

Fig 3. Time-averaged and area-averaged WSSAG and OSI for normal and damped ECA waveforms over range of ratio of ECA to ICA flow for normal carotid artery bifurcation geometry (see Fig 1, *A*).

putational model has been validated with experimental data sets.[13]

Hemodynamic wall parameters. Because arterial walls are subjected to flow-induced shear stresses that vary with time and location, hemodynamic wall parameters derived from the WSS field are necessary to account for this effect. Two hemodynamic wall parameters were computed: the time-averaged WSS angle gradient (WSSAG),[14] which is a mesh- independent measure of spatial variations in the mean WSS direction, and the oscillatory shear index (OSI).[15,16] Both parameters were derived from local values of the two-component WSS vector. As defined, the OSI and WSSAG are time-averaged and thus represent the effect of pulsatile flow-induced shear forces on the arterial walls.[3] In turn, the local, time-averaged OSI and WSSAG were area-averaged over the entire CCA and ICA walls to compare flow rate and waveform effects on the carotid branches. Total surface areas of the CCA and ICA for the normal carotid artery bifurcation (Fig 1, *A*), distal external carotid occlusion (Fig 1, *B*), and proximal stump carotid occlusion (Fig 1, *C*) are the same. Total surface area for the external carotid occlusion geometry without the ECA (Fig 1, *D-F*) are smaller than those with the ECA (Fig 1, *A-C*). The magnitude of WSSAG has a maximum, and the magnitude of the WSS is near zero in regions of flow separation and flow reattachment.[14] Elevated WSSAG may lead to changes in endothelial cell architecture, increase in cell turnover linked to enhanced wall permeability, and development of arterial disease at particular sites.[17] The OSI is formed by the ratio of the absolute value of the time-integrated WSS divided by the absolute value of the WSS, integrated over time. Its value ranges from zero to 0.5. Critical threshold values for any of the hemodynamic wall parameters, eg, WSSAG and OSI, have not been fully established. For geometric measurements that contain an open or occluded ECA segment (Fig 1, *A-C*), the ECA and the flow divider walls were omitted from the area-averaged WSSAG and OSI calculations to make valid comparisons of effects on the CCA plus ICA walls. The flow divider typically exhibits high focal WSS values and limited adaptive changes.

RESULTS

ECA flow and waveform. When ECA flow is increased from zero to 151 mL/min, area-averaged WSS increases in the CCA, from 3.0 to 4.4 dynes/cm^2 (46%), and in the ICA, from 16.5 to 17.1 dyne/cm^2 (4%). However, minimum local WSS in the carotid sinus remained much less than 1 dyne/cm^2. Values for WSSAG and OSI area averaged over the CCA and ICA for the range of ECA flow and waveforms are shown in Fig 3. WSSAG increased by 52%, and OSI increased by 144%, with increasing ECA flow and normal waveform. Damping of the ECA waveform had little effect on area-averaged WSSAG, but it lowered OSI to an overall 68% increase. Local values for WSS, WSSAG, and OSI along the CCA and ICA wall opposite the flow divider are shown in Fig 4. WSS approaches zero in the carotid bulb. Maximum local values for WSSAG and OSI occur in the carotid sinus and increase

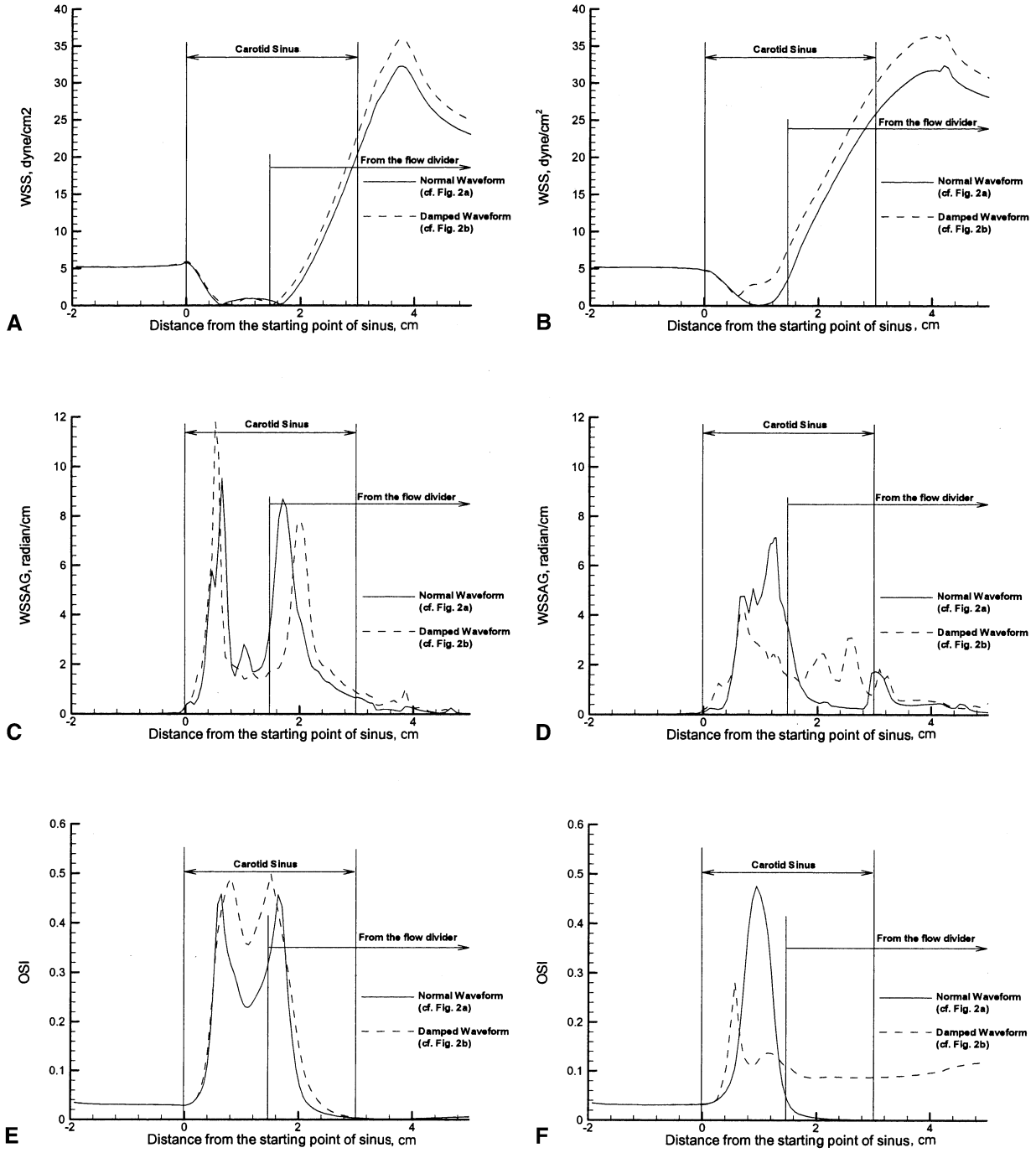

Fig 4. Distribution of time-averaged local values for WSS, WSSAG, and OSI along walls opposite flow divider for a normal carotid bifurcation (see Fig 1, *A*) with normal (*solid lines*) and damped (*dashed lines*) flow waveforms. **A**, CCA-ICA WSS distribution. **B**, CCA-ECA WSS distribution. **C**, CCA-ICA WSSAG distribution. **D**, CCA- ECA WSSAG distribution. **E**, CCA-ICA OSI distribution. **F**, CCA-ECA OSI distribution.

from 3.5 to 9.1 radian/cm (160%) and 0.23 to 0.46 (100%), respectively.

ECA occlusion. Time-averaged local hemodynamic wall parameters, ie, WSS, WSSAG, and OSI, along the CCA and ICA walls opposite the divider in the symmetry plane are shown in Fig 5. These results are for a normal ICA waveform with no ECA flow. WSS, WSSAG, and OSI distributions for distal occlusion geometry and proximal

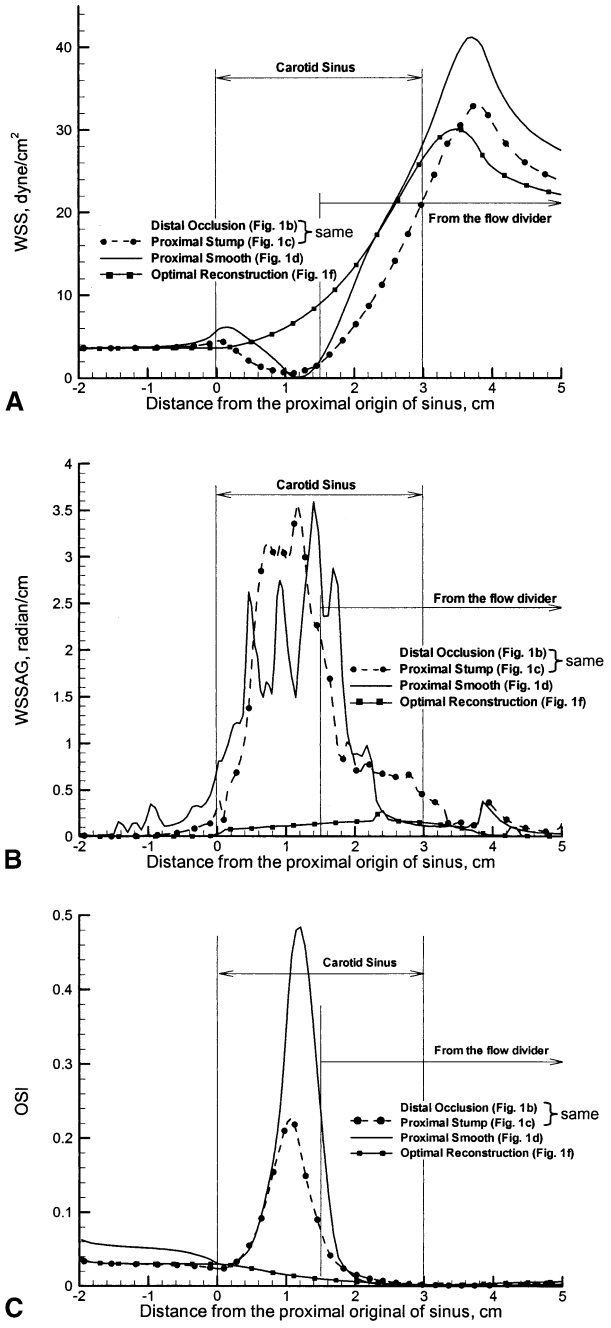

Fig 5. Distribution of time-averaged local values for WSS, WSSAG, and OSI along CCA and ICA walls opposite the divider when ECA is occluded.

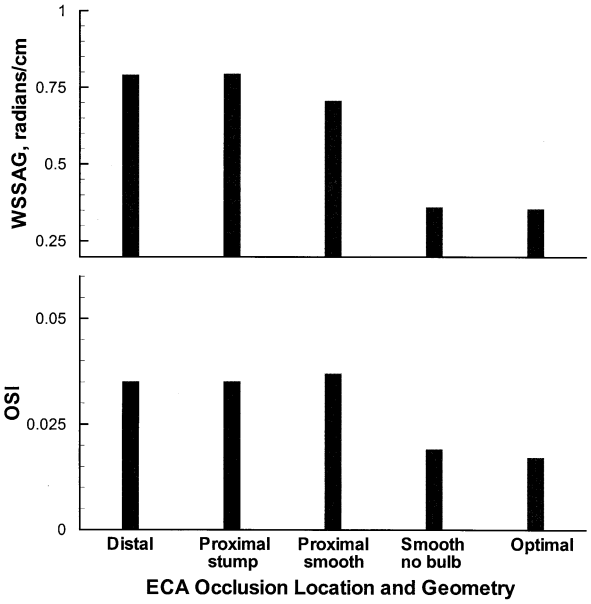

Fig 6. WSSAG and OSI values for five ECA occlusion geometry studies shown in Fig 1, *B-F*.

stump geometry (Fig 1, B and C) are almost identical, and are shown by single curves in Fig 5. When the carotid geometry is normal, WSS is near zero in the carotid sinus, but when the sinus is removed or the geometry is hemodynamically optimized, the minimum local WSS is approximately 4 dynes/cm^2. Similarly, eliminating the carotid sinus markedly reduces local maximum WSSAG from 3.0 to 3.5 radian/cm to 0.3 radians/cm, and local maximum OSI values in the range of 0.22 to 0.49 are reduced to 0.04. Time-averaged and area-averaged WSSAG and OSI over the entire CCA and ICA walls for the five ECA occlusions shown in Fig 1 are presented in Fig 6. WSSAG decreases from 0.793 radian/cm for distal and proximal stump occlusion to 0.361 radian/cm for a smooth occlusion without the carotid sinus, to 0.350 radian/cm when the geometry is optimal. OSI is essentially unchanged at 0.037 to 0.035 for three occlusions, and decreases to 0.019 when the bulb is eliminated and to 0.017 when the geometry is optimized.

DISCUSSION

There are two major findings of this study. First, there is a high near linear dependence of WSSAG and OSI on ECA flow. Increasing ECA flow from zero to 64% of ICA flow increases CCA and ICA area-averaged WSSAG approximately by 50% and triples area-averaged OSI. Local WSS values are lowest and local WSSAG and OSI values are highest in the carotid sinus. Second, when the ECA is occluded, WSS, WSSAG, and OSI are relatively insensitive to the location of ECA occlusion. However, a smooth ECA occlusion flush with the CCA and ICA walls and removal of the carotid sinus markedly reduces local and area-averaged WSSAG and OSI. This occlusion geometry also elevates the minimum local WSS values from zero to more than 4 dynes/cm^2.

Other arterial branching systems with discordant waveforms, flow, and geometry, including the renal, celiac, and hepatic arteries, may be hemodynamically adversely affected similarly to the way carotid bulb flow is affected by the ECA. Renal artery stenosis with and without infrarenal aortic stenosis is perhaps the best example. Resting aortic

flow is biphasic, like that in the ECA, whereas renal artery flow has a damped high diastolic waveform similar to that in the ICA.

These ECA flow results are based on single carotid bifurcation geometry and therefore may be somewhat different if other occlusion geometry is used. The observation of variation in disease location[18] and computational hemodynamic analysis results with the carotid geometry is well described.[8,19,20] However, it is likely that the same general trends in direction of WSSAG and OSI with variable ECA flow and occlusion geometry would be produced by other generally acceptable carotid bifurcation geometries.

ECA occlusion without otherwise changing the carotid artery bifurcation geometry improves hemodynamics. The best theoretical hemodynamic outcome is obtained with a smooth ECA occlusion combined with removal of the carotid sinus. While these computational data may not be clinically applicable until correlative clinical or morphologic data become available, these findings raise interesting questions concerning the invasive management of carotid artery disease. For example, is the optimal reconstruction after carotid endarterectomy closure of the origin of the ECA and streaming the transition from CCA to ICA to remove the carotid bulb? Is the optimal carotid stent a tapered one that achieves the same goal? When the ECA has occlusive disease in its early branches, making the odds of successful blind partial eversion ECA only moderate, is leaving the ECA disease intact a viable option?

Results of this computational study strongly suggest clinical evaluation of the role of the ECA on development of occlusive atherosclerosis in the carotid bifurcation, as well as studies on the effect of residual ECA stenosis on CCA and ICA restenosis after CEA and catheter-based angioplasty and stenting. Final recommendations regarding the best invasive treatment of occlusive disease in the carotid artery bifurcation remain open until the role of ECA is further correlated with clinical and morphologic data.

REFERENCES

1. Zarins CK, Giddens DP, Bharadvaj BK, Sottiurai VS, Mabon RF, Glagov S. Carotid bifurcation atherosclerosis: Quantitative correlation of plaque localization with flow velocity profiles and wall shear stress. Circ Res 1983;53:502-14.
2. Ku DN, Giddens DP, Zarins CK, Glagov S. Pulsatile flow and atherosclerosis in the human carotid bifurcation: Positive correlation between plaque location and low and oscillating shear stress. Atherosclerosis 1985;5:293-302.
3. Kleinstreuer C, Hyun S, Buchanan JR, Longest PW, Archie JP Jr, Truskey GA. Hemodynamic parameters and early intimal thickening in branching blood vessels. Crit Rev Biomed Eng 2001;29:1-64.
4. Boysen G, Engell HC. The effect of induced hypertension on internal carotid artery pressure and regional cerebral blood flow during temporary clamping for endarterectomy. Neurology 1972;22:1133-44.
5. Archie JP. The outcome of external carotid endarterectomy during routine carotid endarterectomy. J Vasc Surg 1998;28:585-90.
6. Ascer E, Gennaro M, Pollina RM, Salles-Cunha S, Lorenson E, Yorkovich WR, et al. The natural history of the external carotid artery after carotid endarterectomy: Implications for management. J Vasc Surg 1996;23:582-6.
7. Bharadvaj BK, Mabon RF, Giddens DP. Steady flow in a model of the human carotid bifurcation. II: Laser-Doppler anemometer measurements. J Biomech 1982;15:363-78.
8. Milner JS, Moore JA, Rutt BK, Steinman DA. Hemodynamics of human carotid artery bifurcation: Computational studies with models reconstructed from magnetic resonance imaging of normal subjects. J Vasc Surg 1998;27:143-56.
9. Macosko RA. Rheology: Principles, measurements, and applications. New York: VCH Publications; 1994.
10. CFX-4 users manuals for version 4.4. Pittsburgh, Pa: AEA Technology; 1997.
11. Lonsdale RD. An algebraic multigrid solver for the Navier-Stokes equations on unstructured meshes. Int J Num Meth Heat Fluid Flow 1993;3:3-14.
12. Patankar SV. Numerical heat transfer and fluid flow. Washington, DC: Hemisphere Publishing; 1980.
13. Hyun S, Kleinstreuer C, Archie JP. Hemodynamics analyses of arterial expansions with implications to thrombosis and restenosis. Med Eng Phys 2000;22:13-27.
14. Hyun S, Kleinstreuer C, Archie JP. Computational particle hemodynamics analysis and geometric reconstruction after carotid endarterectomy. Comp Biol Med 2001;31:365-84.
15. He X, Ku D. Pulsatile flow in the human left coronary artery bifurcation: Average conditions. ASME J Biomech Eng 1996;118:74-82.
16. Botnar R, Rappitsch G, Scheidegger MB, Liepsch D, Perktold K, Boesiger P. Hemodynamics in the carotid artery bifurcation: A comparison between numerical simulations and in vitro MRI measurements. J Biomech 2000;33:137-44.
17. Malek AM, Alper SL, Izumo S. Hemodynamic shear stress and its role in atherosclerosis. JAMA 1999;82:2035-42.
18. Fisher M, Fieman S. Geometric factors of the bifurcation in carotid atherogenesis. Stroke 1990;21:267-71.
19. Perktold K, Peter RO, Resch M, Langs G. Pulsatile non-Newtonian blood flow in three-dimensional carotid bifurcation models: A numerical study of flow phenomena under different bifurcation angles. J Biomed Eng 1991;13:507-15.
20. Wells DR, Archie JP, Kleinstreuer C. Effects of carotid artery geometry on the magnitude and distribution of wall shear stress gradients. J Vasc Surg 1996;23:667-78.

Submitted Jan 8, 2002; accepted Oct 31, 2002.